CHEMISTRY OF MATERIALS

Article

pubs.acs.org/cm

High-Performance Formamidinium-Based Perovskite Solar Cells via Microstructure-Mediated δ-to-α Phase Transformation

Tanghao Liu,[†,‡,∥] Yingxia Zong,[‡,§] Yuanyuan Zhou,[*,‡] Mengjin Yang,[∥] Zhen Li,[∥] Onkar S. Game,[‡] Kai Zhu,[*,∥] Rui Zhu,[*,†,⊥,#] Qihuang Gong,[†,⊥,#] and Nitin P. Padture[‡]

[†]State Key Laboratory for Artificial Microstructure and Mesoscopic Physics, School of Physics, Peking University, Beijing 100871, China

[‡]School of Engineering, Brown University, Providence, Rhode Island 02912, United States

[§]College of Chemistry and Molecular Engineering, Qingdao University of Science and Technology, Qingdao 266042, P. R. China

[∥]Chemistry and Nanoscience Center, National Renewable Energy Laboratory, Golden, Colorado 80401, United States

[⊥]State Key Laboratory for Mesoscopic Physics, Collaborative Innovation Center of Quantum Matter, School of Physics, Peking University, Beijing 100871, P. R. China

[#]Collaborative Innovation Center of Extreme Optics, Shanxi University, Taiyuan, Shanxi 020006, P. R. China

Supporting Information

ABSTRACT: The $\delta \rightarrow \alpha$ phase transformation is a crucial step in the solution-growth process of formamidinium-based lead triiodide ($FAPbI_3$) hybrid organic–inorganic perovskite (HOIP) thin films for perovskite solar cells (PSCs). Because the addition of cesium (Cs) stabilizes the α phase of $FAPbI_3$-based HOIPs, here our research focuses on $FAPbI_3$(Cs) thin films. We show that having a large grain size in the δ-$FAPbI_3$(Cs) non-perovskite intermediate films is essential for the growth of high-quality α-$FAPbI_3$(Cs) HOIP thin films. Here grain coarsening and phase transformation occur simultaneously during the thermal annealing step. A large starting grain size in the δ-$FAPbI_3$(Cs) thin films suppresses grain coarsening, precluding the formation of voids at the final α-$FAPbI_3$(Cs)–substrate interfaces. PSCs based on the interface void-free α-$FAPbI_3$(Cs) HOIP thin films are much more efficient and stable in the ambient atmosphere. This interesting finding inspired us to develop a simple room-temperature aging method for preparing coarse-grained δ-$FAPbI_3$(Cs) intermediate films, which are subsequently converted to coarse-grained, high-quality α-$FAPbI_3$(Cs) HOIP thin films. This study highlights the importance of microstructure meditation in the processing of formamidinium-based PSCs.

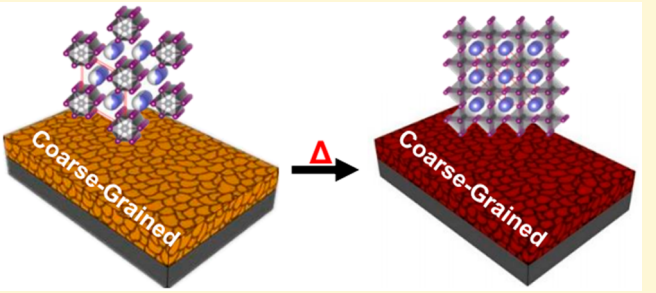

Since the invention of perovskite solar cells (PSCs) in 2009,[1] tremendous research efforts have been devoted to improving the power conversion efficiency (PCE) and stability of PSCs.[2,3] While methylammonium lead triiodide ($CH_3NH_3PbI_3$ or $MAPbI_3$) hybrid organic–inorganic perovskite (HOIP) is the most widely studied for PSC application, it has an intrinsic limitation in harvesting near-infrared (NIR) light in the solar spectrum because of its relatively wide bandgap of ~1.55 eV.[3−5] In addition, the thermal stability of $MAPbI_3$ is a matter of concern considering its low formation entropy.[6] Recently, there has been growing interest in exploring the potential of formamidinium lead triiodide (α-$FAPbI_3$) HOIP for PSC application.[7,8] α-$FAPbI_3$ HOIP has a lower bandgap (~1.45 eV),[9,10] which is closer to the ideal bandgap (1.2−1.3 eV)[11] for single-junction solar cells. Moreover, significantly enhanced thermal stability has been confirmed in α-$FAPbI_3$ as compared to $MAPbI_3$.[12] In spite of these exceptional advantages, there is significant concern about the phase stability of α-$FAPbI_3$, which has held back the development of α-$FAPbI_3$-based PSCs.[13−16] Pure $FAPbI_3$ has two polymorphs at room temperature (RT): the "black" HOIP phase α-$FAPbI_3$ (space group $P3m1$[9,10] or $Pm\bar{3}m$[17]) and the "yellow" non-perovskite phase δ-$FAPbI_3$ (space group $P6_3mc$[9,10]). In some previous studies by some of us[13,16,18] and others,[14,15] it has been shown that the phase transformation (either $\alpha \rightarrow \delta$ or $\delta \rightarrow \alpha$) behavior is closely associated with the degradation and crystallization process of α-$FAPbI_3$ HOIP. The manipulation of such phase transformation is key to the quality of the final α-$FAPbI_3$ HOIP thin films and the performance (PCE and stability) of the resulting PSCs. To date, there have been several studies aimed at understanding and exploiting these effects.[13−16] For example, doping of $FAPbI_3$ with a small amount of inorganic cesium (Cs) appears to be a promising approach for stabilizing the α phase of $FAPbI_3$-based

Received: February 8, 2017
Revised: March 12, 2017
Published: March 14, 2017

DOI: 10.1021/acs.chemmater.7b00523
Chem. Mater. XXXX, XXX, XXX−XXX

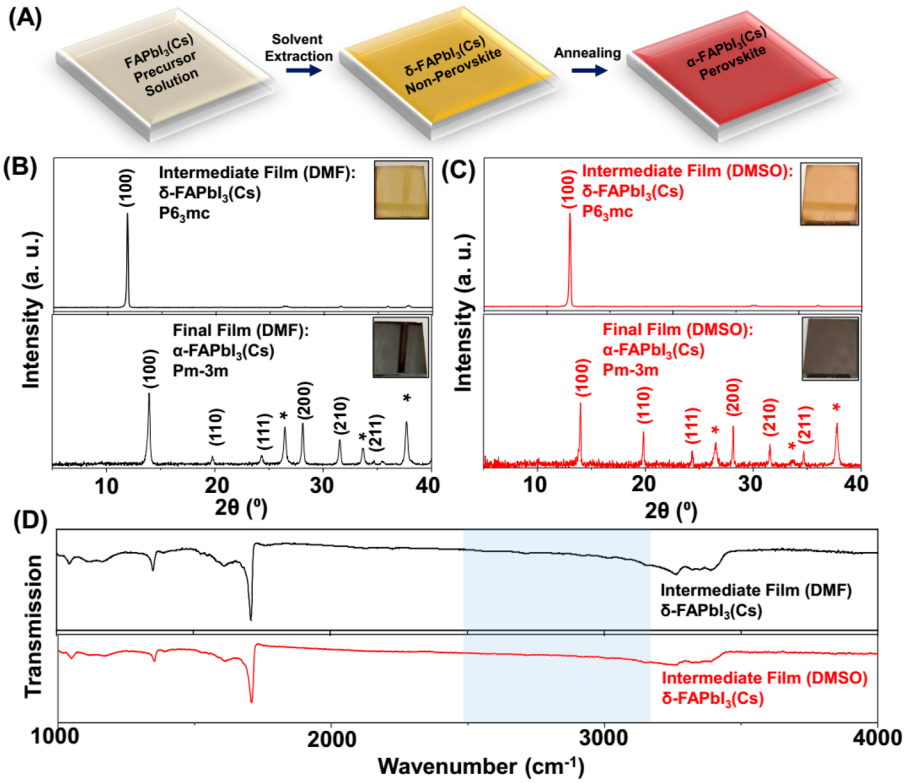

Figure 1. (A) Schematic illustration of the formation process of the α-$FAPbI_3(Cs)$ HOIP thin film. X-ray diffraction patterns of the intermediate and final thin films based on different solvents: (B) dimethylformamide (DMF) and (C) dimethyl sulfoxide (DMSO). Peaks from the substrate are denoted with asterisks. (D) FTIR spectra of the intermediate thin films with either DMF or DMSO as the solvent used in the precursor solutions.

HOIPs.[14−16] [Because of the uncertainty in the actual amount of the Cs incorporated into the HOIP crystal structure, the $FAPbI_3(Cs)$ nomenclature is adopted throughout this paper.] The superior material properties of α-$FAPbI_3(Cs)$ HOIPs and the performance of the resulting PSCs have been unambiguously demonstrated by several groups.[14−16] However, the solution crystallization behavior of α-$FAPbI_3(Cs)$ has been rarely discussed, and the rational selection of specific solvents for the solution synthesis of high-quality α-$FAPbI_3(Cs)$ HOIP thin films has not been elucidated.

In this study, we show that the solution crystallization process of α-$FAPbI_3(Cs)$ HOIP thin films is quite different from that of the widely studied $MAPbI_3$ HOIP films.[19] The antisolvent−solvent extraction (ASE)-based "one-step" method is used here, as this method represents a "model" technique for the growth of uniform HOIP thin films from solution over a wide compositional space.[20−23] Figure 1A schematically shows the crystallization process of α-$FAPbI_3(Cs)$ HOIP thin films. It appears that the first phase that evolves at room temperature (RT) in the ASE process is the "yellow" non-perovskite δ phase. Here, two commonly used solvents, dimethylformamide (DMF) and dimethyl sulfoxide (DMSO) are used in the precursor solutions. The selection of solvent does not affect the phase evolution in the ASE process. As seen in panels B and C of Figure 1, in both cases, phase-pure, highly textured (100) "yellow" δ-$FAPbI_3(Cs)$ thin films are formed at the end of the ASE process. The 100 texture development in the thin film could be the result of the intrinsic one-dimensional (1D) crystallographic symmetry of the δ phase.[9] For comparison, it is well-known that, in the ASE deposition of $MAPbI_3$, some coordinative solution solvents such as DMSO have very strong interactions with $MAPbI_3$, which results in the formation of a large lattice parameter $MAPbI_3 \bullet x$DMSO complex as the first crystalline phase after the ASE process.[19,20] However, both panels B and C of Figure 1 show featureless X-ray diffraction (XRD) patterns in the small-angle region ($2\theta < 10°$), which indicates that the possible $FAPbI_3(Cs) \bullet x$DMF or $FAPbI_3(Cs) \bullet x$DMSO complexes do not form at the end of the ASE process. The Fourier transform infrared spectroscopy (FTIR) results in Figure 1D further confirm the absence of C═O and S═O bonds in the "yellow" δ-$FAPbI_3(Cs)$ intermediate thin films; such bonds are typically present in the complexes.[24] While the detailed chemistry remains to be further elucidated, this interesting difference between $FAPbI_3(Cs)$ and $MAPbI_3$ can be attributed to the unique polymorphism in the former. It is possible that the formation energy of the δ phase is much lower than that of the solvent-coordinated HOIP complexes at low temperatures, which favors the crystallization of δ-$FAPbI_3(Cs)$ as the intermediate phase. Because δ-$FAPbI_3(Cs)$ is energetically not stable at higher temperatures, it turns dark in the subsequent thermal annealing (150 °C) step. Finally, phase-pure α-$FAPbI_3(Cs)$ HOIP films form in both DMF and DMSO cases, as confirmed by the optical photographs and the XRD patterns in panels B and C of Figure 1.

While phases of the intermediate thin films after the ASE have been confirmed above, morphologies of these δ-$FAPbI_3(Cs)$ thin films are then studied using scanning electron microscopy (SEM). Panels A and B of Figure 2 compare the surface morphology of the intermediate δ-$FAPbI_3(Cs)$ thin films prepared using DMF and DMSO, respectively, as solvents in precursor solutions. Average grain sizes of both intermediate δ-$FAPbI_3(Cs)$ thin films are measured with the image analysis approach, and the results are shown in Figure S1. The average grain sizes in the DMF and DMSO cases are ~50 and ~200

DOI: 10.1021/acs.chemmater.7b00523
Chem. Mater. XXXX, XXX, XXX−XXX

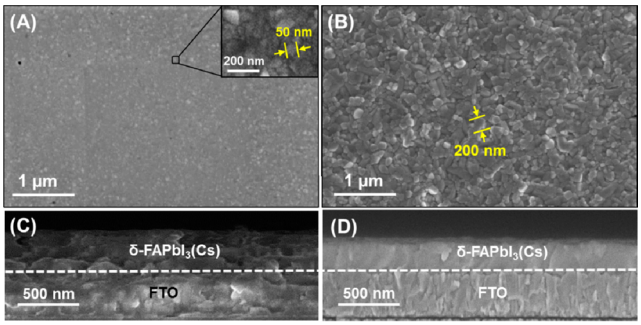

Figure 2. (A and B) Top-view and (C and D) cross-sectional SEM images of the "yellow" δ-$FAPbI_3(Cs)$ non-perovskite intermediate thin film processed using (A and C) DMF and (B and D) DMSO as the solvents in precursor solutions.

nm, respectively. This grain size difference may be related to solvent extraction kinetics in different solvent systems.[25] DMF, which generally has weaker interaction with the halide precursor phases, is assumed to be extracted more rapidly. Thus, a higher degree of supersaturation and a higher nucleation density are expected, which is responsible for the ultrafine grain structure in the as-crystallized δ-$FAPbI_3(Cs)$ thin films. In spite of the grain size difference, the corresponding cross-sectional SEM images of the δ-$FAPbI_3(Cs)$ intermediate thin films in panels C and D of Figure 2 show uniform thickness, excellent compactness, and defect-free film−substrate interfaces in both cases. The smooth, mirrorlike surfaces of "yellow" δ-$FAPbI_3(Cs)$ thin films appear to be retained throughout the process of conversion to the final "black" α-$FAPbI_3(Cs)$ HOIP in both DMF and DMSO cases, as shown in Figure S2. Full coverage and uniform grain structure in α-$FAPbI_3(Cs)$ thin films in both cases are confirmed by the top-view SEM images in panels A and B of Figure 3. Average grain

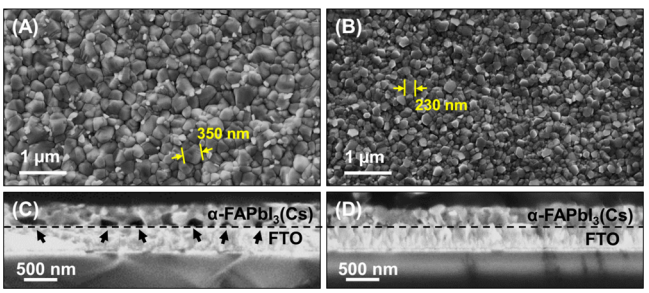

Figure 3. (A and B) Top-view and (C and D) cross-sectional SEM images of the "black" α-$FAPbI_3(Cs)$ HOIP thin films processed using (A and C) DMF and (B and D) DMSO as the solvents in precursor solutions.

sizes of both α-$FAPbI_3(Cs)$ thin films are measured with the image analysis approach, and the results are presented in Figure S3. Average grain sizes of the α-$FAPbI_3(Cs)$ thin films in DMF and DMSO cases are ~350 and ~230 nm, respectively. In this context, a significant grain-coarsening effect is observed in the DMF case (from ~50 to ~350 nm) but not in the DMSO case (from ~200 to ~230 nm). After the phase transformation, the shape of the grains becomes more equiaxed in the α-$FAPbI_3(Cs)$ HOIP thin films, which can be attributed to the three-dimensional "cubic" crystal symmetry[9] of the α-$FAPbI_3(Cs)$. Panels C and D of Figure 3 show cross-sectional SEM images of the α-$FAPbI_3(Cs)$ HOIP thin films processed using DMF and DMSO as solvents in precursor solutions, respectively. Interestingly, in the DMF solvent case, although the top surface of the resultant α-$FAPbI_3(Cs)$ thin film is dense, voids are frequently observed at the α-$FAPbI_3(Cs)$−substrate interface. Because these interfacial defects do not exist in the intermediate δ-$FAPbI_3(Cs)$ thin film (Figure 2C), they appear to emerge during the thermal annealing step. In contrast, in the DMSO solvent case (Figure 2D), the defect-free δ-$FAPbI_3(Cs)$−substrate interface is inherited by the final α-$FAPbI_3(Cs)$ film (Figure 3D), where no defect forms during the thermal annealing step.

On the basis of these phase and microstructure characterization results, a hypothesized mechanism responsible for such differences is schematically shown in Figure 4. Typically, the

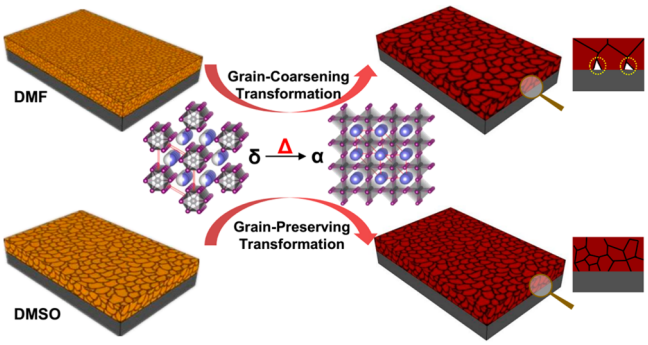

Figure 4. Hypothesized mechanisms for microstructural evolution associated with the δ-to-α phase transformation during thermal annealing. Note that "grain-preserving" here means there is no obvious coarsening of grains during the phase transformation.

thermal annealing treatment simultaneously induces two effects: $\delta \rightarrow \alpha$ phase transformation and grain coarsening. The grain-coarsening behavior is described by the equation $d^2 - d_0^2 = Kt$, where d_0 is the initial grain size, d is the final grain size, t is the time, and K is a constant with exponential temperature dependence.[19,26] In the DMF solvent case, the grain size in the final α-$FAPbI_3(Cs)$ HOIP thin film is ~7 times of that in the starting δ-$FAPbI_3(Cs)$ thin film. By contrast, in the DMSO case, the grain size does not change much. Moreover, the phase transformations in the two cases reach completion at almost the same time (Figure S2). Therefore, the grain coarsening rate in the DMF solvent case is much higher than that in the DMSO solvent case. Such a rapid change in the microstructure together with the phase transformation may increase the possibility of the generation of voids. Note that, compared with the top surface and interior of the thin film, the film−substrate interface is less accommodating of significant changes in the thin film microstructure because of the substrate constraint, which may explain the appearance of voids at the α-$FAPbI_3(Cs)$−substrate interface. In the case of the DMSO solvent, the grain coarsening during the phase transformation is negligible, resulting in a relatively stable microstructure, mitigating the formation of defects at the α-$FAPbI_3(Cs)$−substrate interface.

To evaluate the photovoltaic (PV) performance of the α-$FAPbI_3(Cs)$ HOIP thin films, a planar PSC architecture with the HOIP thin film sandwiched between an electron-extracting TiO_2/FTO (fluorinated tin oxide) anode and a hole-extracting spiro-OMeTAD/Ag cathode is employed. Figure 5A shows the typical current density (J)−voltage (V) curves (reverse scans) of PSCs based on α-$FAPbI_3(Cs)$ HOIP films processed using

DOI: 10.1021/acs.chemmater.7b00523
Chem. Mater. XXXX, XXX, XXX−XXX

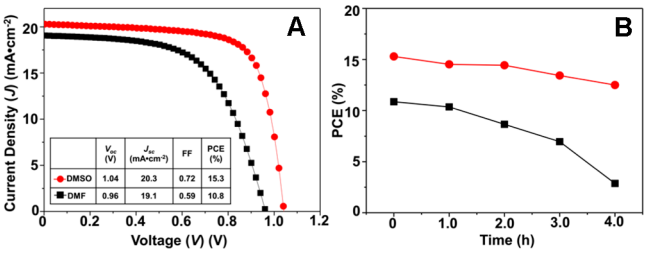

Figure 5. Planar PSCs based on $FAPbI_3(Cs)$ thin films processed using DMF (black) and DMSO (red) as solvents in the precursor solutions: (A) $J-V$ responses (inset, PV performance parameters) and (B) ambient stability of PCE.

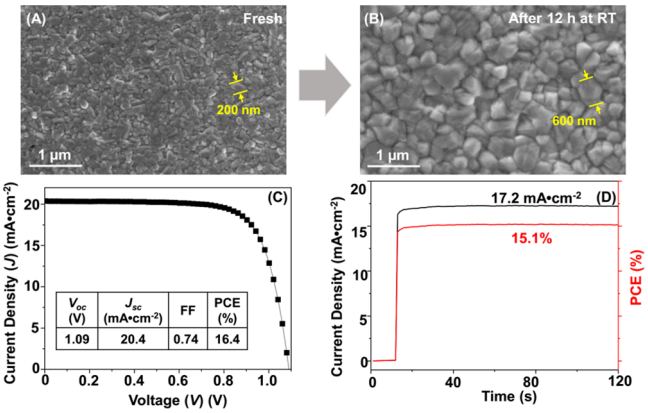

Figure 6. Top-view SEM images of a δ-$FAPbI_3(Cs)$ thin film processed using DMSO as the solvent: (A) before and (B) after additional 12 h room-temperature aging. (C) Current density–voltage ($J-V$) response (inset, PV performance parameters) of the PSC based on the α-$FAPbI_3(Cs)$ HOIP thin film converted from the coarse-grained δ-$FAPbI_3(Cs)$ thin film. (D) Stabilized J and PCE output at the maximal power point (V = 0.88 V).

DMF and DMSO as solvents in precursor solutions. The respective PV performance parameters extracted from $J-V$ curves are shown in the inset table of Figure 5A. It is clear that the PSC processed with DMSO solvent shows much better PV performance with respect of all PV parameters. The typical PCE (15.3%) in the DMSO case is 50% higher than that in the DMF case (10.8%). Figure S4 shows that $J-V$ hysteresis exists in both cases. While the hysteresis is typical in the TiO_2-based planar PSCs, the PSC processed with the DMSO solvent shows significantly suppressed hysteresis. These superior PV performance parameters can be clearly attributed to the absence of the interfacial defects in the α-$FAPbI_3(Cs)$ HOIP thin films processed using the DMSO solvent. The voids observed in Figure 3C at the α-$FAPbI_3(Cs)$ thin film–substrate interface in the DMF case are detrimental to photogenerated carrier extraction. With regard to the ambient stability, the unstable nature of the PSC processed using the DMF solvent can even be witnessed by the naked eye. The "black" α-$FAPbI_3(Cs)$ HOIP thin film, despite being sandwiched by the anode and cathode, is bleached within 4 h (see Figure S5) in the ambient atmosphere (temperature of ~25 °C, relative humidity of ~40%). The rapid degradation of the α-$FAPbI_3(Cs)$ HOIP thin film and the corresponding device performance (Figure 4B) can be attributed to the interfacial voids that allow easy ingression of moisture into the PSC at the interface. In contrast, in the DMSO solvent case, the PSC still maintains >80% of its initial PCE after being exposed to the same ambient conditions for 4 h (Figure 5B).

The microstructure-mediated $\delta \rightarrow \alpha$ phase transformation has several advantages in the fabrication of high-performance $FAPbI_3(Cs)$-based PSCs. However, the grain size of the final α-$FAPbI_3(Cs)$ HOIP thin film is limited by the δ-$FAPbI_3(Cs)$ non-perovskite intermediate thin film. HOIP thin films with larger grains are generally beneficial for PSC operation because of the reduced grain boundary density.[27] To form a coarse-grained α-$FAPbI_3(Cs)$ thin film, the as-formed δ-$FAPbI_3(Cs)$ intermediate thin film (processed with DMSO) is stored at RT in a closed Petri dish for 12 h. This simple step leads to the coarsening of δ-$FAPbI_3(Cs)$ grains from ~200 to ~600 nm without δ-to-α phase transformation.[28,29] The surface morphologies of the fresh and aged δ-$FAPbI_3(Cs)$ thin films are compared in panels A and B of Figure 6. The compact nature of the δ-$FAPbI_3(Cs)$ thin film is retained after the RT coarsening process (Figure S7A). After conversion to α-$FAPbI_3(Cs)$, the grain size is still ~600 nm (Figure S6), which is much larger than that (~230 nm) in the non-aged α-$FAPbI_3(Cs)$ HOIP thin film (Figure 3B). Besides, the HOIP–substrate interface retains its defect-free nature (Figure S7B), making it suitable for PV application. Taking advantage of the larger grain size in the final HOIP film, the relevant PSC shows a further enhanced PCE of 16.4% (Figure 6C). The stabilized output at the maximal power point (V = 0.88 V) shows a PCE of 15.1% under 1 sun illumination (Figure 6D). The incident photon-to-current conversion efficiency (IPCE) spectrum was also recorded for this device (Figure S8), showing an integrated J_{sc} of 19.9 mA/cm^2, approaching the value extracted from the $J-V$ curve. Further effort is underway to achieve even larger-grained δ-$FAPbI_3(Cs)$ starting thin films for the "grain-preserving" $\delta \rightarrow \alpha$ phase transformation process, which will lead to more efficient, stable PSCs.

In closing, we have shown that $\delta \rightarrow \alpha$ phase transformation has a profound impact on the morphology and microstructure of the final α-$FAPbI_3(Cs)$ HOIP thin films, as well as the PV performance of the resulting PSCs. By simply changing the precursor solution solvent (DMF or DMSO) and performing simple RT aging, we can tailor the microstructures of the intermediate δ-$FAPbI_3(Cs)$ non-perovskite thin film. Large-grained δ-$FAPbI_3(Cs)$ thin films favor conversion to defect-free and large-grained α-$FAPbI_3(Cs)$ HOIP thin films via a microstructure-mediated process. PSCs based on these HOIP thin films show high efficiency and stability. The observations and insights provided in this study have profound implications for the understanding of the $\delta \rightarrow \alpha$ phase transformation of formamidinium-based HOIPs. It is worth noting that while $FAPbI_3(Cs)$ is studied as a representative composition in this study, similar behavior can be expected in other formamidinium-based compositions. In the future, we envision that more effort will be devoted to decoupling the steps mentioned above for accurate control of phase transformation of formamidinium-based HOIP thin films, resulting in PSCs with further enhanced performance and stability.

■ ASSOCIATED CONTENT

Supporting Information

The Supporting Information is available free of charge on the ACS Publications website at DOI: 10.1021/acs.chemmater.7b00523.

Experimental procedures, Figures S1–S8, and two references (PDF)

DOI: 10.1021/acs.chemmater.7b00523
Chem. Mater. XXXX, XXX, XXX–XXX

AUTHOR INFORMATION

Corresponding Authors

*E-mail: yuanyuan_zhou@brown.edu.
*E-mail: Kai.Zhu@nrel.gov.
*E-mail: iamzhurui@pku.edu.cn.

ORCID

Kai Zhu: 0000-0003-0908-3909

Notes

The authors declare no competing financial interest.

ACKNOWLEDGMENTS

T.L., Y. Zong, O.S.G., and N.P.P. thank the National Science Foundation (Grants DMR-1305913 and OIA-1538893) for the funding for the research performed at Brown University. T.L., R.Z., and Q.G. acknowledge the funding from the 973 Program of China (2015CB932203), the National Natural Science Foundation of China (61377025, 91433203, and 11121091), and the Young 1000 Talents Global Recruitment Program of China. M.Y., Z.L., and K.Z. acknowledge the support by the hybrid perovskite solar cell program of the National Center for Photovoltaics funded by the U.S. Department of Energy (DOE), Office of Energy Efficiency and Renewable Energy (EERE), Solar Energy Technologies Office (SETO), for the funding for the research performed at the National Renewable Energy Laboratory (DE-AC36-08-GO28308).

REFERENCES

(1) Kojima, A.; Teshima, K.; Shirai, Y.; Miyasaka, T. Organometal Halide Perovskites as Visible-Light Sensitizers for Photovoltaic Cells. *J. Am. Chem. Soc.* **2009**, *131*, 6050−6051.

(2) http://www.nrel.gov/pv/assets/images/efficiency_chart.jpg.

(3) Stranks, S. D.; Snaith, H. J. Metal-halide perovskites for photovoltaic and light-emitting devices. *Nat. Nanotechnol.* **2015**, *10*, 391−402.

(4) Zhou, Y.; Zhu, K. Perovskite Solar Cells Shine in the "Valley of the Sun. *ACS Energy Lett.* **2016**, *1*, 64−67.

(5) Jeon, N. J.; Noh, J. H.; Yang, W. S.; Kim, Y. C.; Ryu, S.; Seo, J.; Seok, S. I. Compositional engineering of perovskite materials for high-performance solar cells. *Nature* **2015**, *517*, 476−480.

(6) Nagabhushana, G. P.; Shivaramaiah, R.; Navrotsky, A. Direct calorimetric verification of thermodynamic instability of lead halide hybrid perovskites. *Proc. Natl. Acad. Sci. U. S. A.* **2016**, *113*, 7717−7721.

(7) Zhou, Y.; Zhou, Z.; Chen, M.; Zong, Y.; Huang, J.; Pang, S.; Padture, N. P. Doping and alloying for improved perovskite solar cells. *J. Mater. Chem. A* **2016**, *4*, 17623−17635.

(8) Saliba, M.; Matsui, T.; Domanski, K.; Seo, J.-Y.; Ummadisingu, A.; Zakeeruddin, S. M.; Correa-Baena, J.-P.; Tress, W. R.; Abate, A.; Hagfeldt, A.; Grätzel, M. Incorporation of rubidium cations into perovskite solar cells improves photovoltaic performance. *Science* **2016**, *354*, 206−209.

(9) Stoumpos, C. C.; Malliakas, C. D.; Kanatzidis, M. G. Semiconducting Tin and Lead Iodide Perovskites with Organic Cations: Phase Transitions, High Mobilities, and Near-Infrared Photoluminescent Properties. *Inorg. Chem.* **2013**, *52*, 9019−9038.

(10) Pang, S.; Hu, H.; Zhang, J.; Lv, S.; Yu, Y.; Wei, F.; Qin, T.; Xu, H.; Liu, Z.; Cui, G. $NH_2CH{=}NH_2PbI_3$: An Alternative Organolead Iodide Perovskite Sensitizer for Mesoscopic Solar Cells. *Chem. Mater.* **2014**, *26*, 1485−1491.

(11) Meillaud, F.; Shah, A.; Droz, C.; Vallat-Sauvain, E.; Miazza, C. Efficiency limits for single-junction and tandem solar cells. *Sol. Energy Mater. Sol. Cells* **2006**, *90*, 2952−2959.

(12) Eperon, G. E.; Stranks, S. D.; Menelaou, C.; Johnston, M. B.; Herz, L. M.; Snaith, H. J. Formamidinium lead trihalide: a broadly tunable perovskite for efficient planar heterojunction solar cells. *Energy Environ. Sci.* **2014**, *7*, 982−988.

(13) Zhou, Y.; Kwun, J.; Garces, H. F.; Pang, S.; Padture, N. P. Observation of phase-retention behavior of the $HC(NH_2)_2PbI_3$ black perovskite polymorph upon mesoporous TiO_2 scaffolds. *Chem. Commun.* **2016**, *52*, 7273−7275.

(14) Lee, J.-W.; Kim, D.-H.; Kim, H.-S.; Seo, S.-W.; Cho, S. M.; Park, N.-G. Formamidinium and Cesium Hybridization for Photo- and Moisture-Stable Perovskite Solar Cell. *Adv. Energy Mater.* **2015**, *5*, 1501310.

(15) Yi, C.; Luo, J.; Meloni, S.; Boziki, A.; Ashari-Astani, N.; Gratzel, C.; Zakeeruddin, S. M.; Rothlisberger, U.; Gratzel, M. Entropic stabilization of mixed A-cation ABX3 metal halide perovskites for high performance perovskite solar cells. *Energy Environ. Sci.* **2016**, *9*, 656−662.

(16) Li, Z.; Yang, M.; Park, J.-S.; Wei, S.-H.; Berry, J. J.; Zhu, K. Stabilizing Perovskite Structures by Tuning Tolerance Factor: Formation of Formamidinium and Cesium Lead Iodide Solid-State Alloys. *Chem. Mater.* **2016**, *28*, 284−292.

(17) Weller, M. T.; Weber, O. J.; Frost, J. M.; Walsh, A. Cubic Perovskite Structure of Black Formamidinium Lead Iodide, α-$[HC(NH_2)_2]PbI_3$, at 298 K. *J. Phys. Chem. Lett.* **2015**, *6*, 3209−3212.

(18) Wang, Z.; Zhou, Y.; Pang, S.; Xiao, Z.; Zhang, J.; Chai, W.; Xu, H.; Liu, Z.; Padture, N. P.; Cui, G. Additive-Modulated Evolution of $HC(NH_2)_2PbI_3$ Black Polymorph for Mesoscopic Perovskite Solar Cells. *Chem. Mater.* **2015**, *27*, 7149−7155.

(19) Zhou, Y.; Game, O. S.; Pang, S.; Padture, N. P. Microstructures of Organometal Trihalide Perovskites for Solar Cells: Their Evolution from Solutions and Characterization. *J. Phys. Chem. Lett.* **2015**, *6*, 4827−4839.

(20) Jeon, N. J.; Noh, J. H.; Kim, Y. C.; Yang, W. S.; Ryu, S.; Seok, S. I. Solvent engineering for high-performance inorganic−organic hybrid perovskite solar cells. *Nat. Mater.* **2014**, *13*, 897−903.

(21) Xiao, M.; Huang, F.; Huang, W.; Dkhissi, Y.; Zhu, Y.; Etheridge, J.; Gray-Weale, A.; Bach, U.; Cheng, Y.-B.; Spiccia, L. A Fast Deposition-Crystallization Procedure for Highly Efficient Lead Iodide Perovskite Thin-Film Solar Cells. *Angew. Chem.* **2014**, *126*, 10056−10061.

(22) Zhou, Y.; Yang, M.; Wu, W.; Vasiliev, A. L.; Zhu, K.; Padture, N. P. Room-temperature crystallization of hybrid-perovskite thin films via solvent-solvent extraction for high-performance solar cells. *J. Mater. Chem. A* **2015**, *3*, 8178−8184.

(23) Jesper Jacobsson, T.; Correa-Baena, J.-P.; Pazoki, M.; Saliba, M.; Schenk, K.; Gratzel, M.; Hagfeldt, A. Exploration of the compositional space for mixed lead halogen perovskites for high efficiency solar cells. *Energy Environ. Sci.* **2016**, *9*, 1706−1724.

(24) http://webbook.nist.gov/.

(25) Zhou, Y.; Yang, M.; Game, O. S.; Wu, W.; Kwun, J.; Strauss, M. A.; Yan, Y.; Huang, J.; Zhu, K.; Padture, N. P. Manipulating Crystallization of Organolead Mixed-Halide Thin Films in Antisolvent Baths for Wide-Bandgap Perovskite Solar Cells. *ACS Appl. Mater. Interfaces* **2016**, *8*, 2232−2237.

(26) Kingery, W. D.; Bowen, H. K.; Uhlmann, D. R. *Introduction to Ceramics*, 2nd ed.; Wiley-Interscience: New York, 1976.

(27) Xiao, Z.; Dong, Q.; Bi, C.; Shao, Y.; Yuan, Y.; Huang, J. Solvent Annealing of Perovskite-Induced Crystal Growth for Photovoltaic-Device Efficiency Enhancement. *Adv. Mater.* **2014**, *26*, 6503−6509.

(28) Liu, T.; Hu, Q.; Wu, J.; Chen, K.; Zhao, L.; Liu, F.; Wang, C.; Lu, H.; Jia, S.; Russell, T.; Zhu, R.; Gong, Q. Mesoporous PbI_2 Scaffold for High-Performance Planar Heterojunction Perovskite Solar Cells. *Adv. Energy Mater.* **2016**, *6*, 1501890.

(29) Zhou, Y.; Yang, M.; Kwun, J.; Game, O. S.; Zhao, Y.; Pang, S.; Padture, N. P.; Zhu, K. Intercalation crystallization of phase-pure [small alpha]-$HC(NH_2)_2PbI_3$ upon microstructurally engineered PbI_2 thin films for planar perovskite solar cells. *Nanoscale* **2016**, *8*, 6265−6270.

DOI: 10.1021/acs.chemmater.7b00523
Chem. Mater. XXXX, XXX, XXX−XXX